Swansea University
Prifysgol Abertawe

Cronfa
Setting Research Free

Cronfa - Swansea University Open Access Repository

_____

_____

A novel displacement-based Trefftz plate element with high distortion tolerance for orthotropic thick plates

Yan Shang[1, *], Chen-Feng Li[2], Ming-Jue Zhou[3]

[1]*State Key Laboratory of Mechanics and Control of Mechanical Structures, College of Aerospace Engineering, Nanjing University of Aeronautics and Astronautics, Nanjing 210016, China*

[2]*Zienkiewicz Centre for Computational Engineering and Energy Safety Research Institute, College of Engineering, Swansea University, Swansea SA1 8EN, UK*

[3]*College of Mechanical Engineering, Zhejiang University of Technology, Hangzhou 310017, China*

Abstract

In this work, a simple but robust 4-node displacement-based Trefftz plate element is proposed for efficiently analysis of orthotropic plate structures. This is achieved via two steps. First, the element's deflection and rotation fields are directly formulated at the base of the Trefftz functions of the orthotropic Mindlin-Reissner plate. Second, to ensure the convergence property and further enhance the element performance, the generalized conforming theory is employed to satisfy the requirement for interelement compatibility in weak sense. The resulting displacement-based element belongs to the nonconforming models on coarse meshes and gradually converges into a conforming one with the mesh refinement. Numerical benchmarks reveal that the new element can produce high precision results for both displacement and stress resultant. Moreover, it is free of shear locking and has good tolerances to mesh distortions.

Keywords: Displacement-based Trefftz element; Mindlin-Reissner plate; Generalized conforming; locking free; Mesh distortion

1. Introduction

Due to the superior strength to weight ratio and stiffness to weight ratio, orthotropic plate structures have been widely used in various engineering applications. For well understanding and effectively designing such structures, accurate numerical tools are clearly required, in which the finite element

---

∗Correspondence to: Dr. Yan Shang, State Key Laboratory of Mechanics and Control of Mechanical Structures, College of Aerospace Engineering, Nanjing University of Aeronautics and Astronautics, Nanjing 210016, China
E-mail: shangyan@nuaa.edu.cn

method (FEM) is usually regarded as the most popular choice. In the earlier history, most plate finite elements are developed based on the classical Kirchhoff thin plate theory [1]. However, because the transverse shear deformation is neglected in the Kirchhoff plate theory, these Kirchhoff plate elements are only appropriate for modeling thin structures. In contrast, in Mindlin-Reissner plate theory, the deflection and rotations are independently defined and the transverse shear strain is assumed to be constant through the plate thickness. Thus, the Mindlin-Reissner plate elements can appropriately describe the behaviors of thick plates. Another advantage of the Mindlin-Reissner plate theory is that it is applicable to both thick and thin plates. In addition, there are also some element models developed based on other plate theories, such as the higher order shear deformation theory [2], the zig-zag theory [3-5], etc. These plate theories indeed can provide improved shear deformation responses but at cost of a significant increase in computation expense.

Over the past decades, how to develop high-performance Mindlin-Reissner plate elements has drawn great attentions from scholars in both computation mechanics and computation engineering communities. Various methodologies and schemes have been successfully proposed, such as the enhanced assumed strain (EAS) method [6-9], the smoothed FEM [10-15], the quasi-conforming element method [16-18], the mixed interpolated tensorial components method [19-21], the refined non-conforming element method [22, 23], the high-order linked interpolation method [24, 25], etc. A comprehensive literature review can be found in [26]. Amongst these available approaches, the hybrid-Trefftz finite element method [27-29], which successfully blends the attributes of the Trefftz method [30] with the usual hybrid element method, is a very attractive one. In hybrid-Trefftz element models, the internal displacement or stress trial field is assumed as the sum of the analytical homogeneous solutions and particular solution, namely the Trefftz functions, so that it can a priori satisfy related governing equations. As a benefit, good numerical accuracy can be expected and the challenging shear locking problem can be easily eliminated. Since its inception, the hybrid-Trefftz finite element method has become increasingly popular and been applied to solve various solid mechanics problems [31-37].

However, to our best knowledge, a very few studies have been performed on the topic of the orthotropic thick plates. Among the existing works, Petrolito [38, 39] derived the Trefftz functions of the orthotropic Mindlin-Reissner plate by transforming all governing differential equations into one equation, and then used these Trefftz functions to develop a 3-node triangular hybrid-Trefftz

element for analysis of the orthotropic thick plate structures. Karkon and Rezaiee-Pajand [40] also developed 3-node triangular and 4-node quadrilateral plate elements in an analogous manner. But, it is found that their approach for deriving the Trefftz functions will be inapplicable when the order of Trefftz function exceeds four. More recently, Ray [41] proposed a non-classical hybrid-Trefftz element formulation in which the Trefftz functions are obtained by directly solving the simultaneous governing equations and the particular solution is no longer required.

Comparing with the hybrid element models, the displacement-based elements may be more preferred in practical applications because of some inherent advantages. For instance, the displacement-based elements can be extended to the nonlinear cases more directly [42]. However, it should be noted that the Trefftz functions are generally not compatible across the interface between two neighboring elements. A displacement-only finite element implementation using Trefftz functions will produce non-conforming models whose convergence properties are often queried. Thus, it delivers a question that: whether an efficient and robust displacement-based Trefftz element can be developed for analysis of orthotropic thick plates.

This work aims to propose an answer to the above question. A novel 4-node 12-DOF (degree of freedom) quadrilateral displacement-based Trefftz plate element will be constructed via two steps. First, the polynomial Trefftz solutions of the orthotropic Mindlin-Reissner plate are solved by converting related simultaneous governing equations into three equations. Then, these Trefftz solutions are employed to formulate the element's deflection and rotation fields in a straightforward way. Second, to ensure the convergence property and future improve the element's performance, the generalized conforming theory [43-45] is introduced to meet the requirement for interelement compatibility in weak sense. The resulting generalized conforming Trefftz plate element will perform as a non-conforming model on coarse meshes and gradually converge into the conforming one as the mesh refined.

Several benchmark examples are tested to assess the new element's capability. Numerical results reveal that this new element can produce high precision results for both the displacement and stress resultant in analysis of thin and thick plate structures. Moreover, the proposed new element is free of shear locking and has exceptional tolerances to mesh distortion.

2. Analytical solutions for orthotropic Mindlin-Reissner plate

2.1 Basic governing equations

For orthotropic plates, it's common to firstly describe their behaviors by using a local coordinate system, in which *x*- and *y*- axes are the two material principal directions whilst *z*- denotes the plate thickness direction. As illustrated in Figure 1, in Mindlin-Reissner plate theory, the transverse deflection and rotations are independently defined and can be expressed in the following vector form:

$$\mathbf{u} = \begin{bmatrix} w & \psi_x & \psi_y \end{bmatrix}^{\mathrm{T}}. \tag{1}$$

The bending curvatures and transverse shear strains can be obtained by

$$\boldsymbol{\varepsilon} = \begin{bmatrix} \kappa_x & \kappa_y & \kappa_{xy} & \gamma_x & \gamma_y \end{bmatrix}^{\mathrm{T}} = \mathbf{Lu}, \tag{2}$$

with

$$\mathbf{L} = \begin{bmatrix} 0 & \partial/\partial x & 0 \\ 0 & 0 & \partial/\partial y \\ 0 & \partial/\partial y & \partial/\partial x \\ \partial/\partial x & -1 & 0 \\ \partial/\partial y & 0 & -1 \end{bmatrix}. \tag{3}$$

For linear elastic cases, the constitutive relations between the strain and stress can be generally written as

$$\boldsymbol{\sigma} = \begin{bmatrix} M_x & M_y & M_{xy} & Q_x & Q_y \end{bmatrix}^{\mathrm{T}} = \mathbf{D}\boldsymbol{\varepsilon}, \tag{4}$$

with

$$\mathbf{D} = \begin{bmatrix} \mathbf{D}_b & \\ & \mathbf{D}_s \end{bmatrix}, \tag{5}$$

in which

$$\mathbf{D}_b = \begin{bmatrix} D_x & D_1 & 0 \\ D_1 & D_y & 0 \\ 0 & 0 & D_{xy} \end{bmatrix}, \tag{6}$$

$$\mathbf{D}_s = \begin{bmatrix} C_{xz} & \\ & C_{yz} \end{bmatrix}. \tag{7}$$

Particularly for the single-layer plate composed of orthotropic material, the components of Equation (6) and Equation (7) can be calculated as follows:

$$D_x = \frac{E_x h^3}{12(1-\mu_{xy}\mu_{yx})}, \quad D_y = \frac{E_y h^3}{12(1-\mu_{xy}\mu_{yx})}, \quad D_{xy} = \frac{G_{xy} h^3}{12}, \quad D_1 = \mu_{xy} D_y = \mu_{yx} D_x, \tag{8}$$

$$C_{xz} = k h G_{xz}, \quad C_{yz} = k_s h G_{yz}, \tag{9}$$

where $E_x, E_y, \mu_{xy}, \mu_{yx}, G_{xy}, G_{xz}, G_{yz}$ are the engineering material constants; h denotes the plate thickness; k_s is the shear deformation correction coefficient and usually taken as 5/6.

Besides, the equilibrium equations are given by

$$\begin{cases} \dfrac{\partial M_x}{\partial x} + \dfrac{\partial M_{xy}}{\partial y} + Q_x = 0 \\[2mm] \dfrac{\partial M_{xy}}{\partial x} + \dfrac{\partial M_y}{\partial y} + Q_y = 0 \\[2mm] \dfrac{\partial Q_x}{\partial x} + \dfrac{\partial Q_y}{\partial y} + q = 0 \end{cases} \tag{10}$$

2.2 Analytical solutions of Mindlin-Reissner plate

To derive the analytical solutions of the orthotropic Mindlin-Reissner plate, the next assumptions proposed in [38] are introduced:

$$\psi_x = \frac{\partial w}{\partial x} + \frac{1}{C_{xz}}\left(D_x \frac{\partial^3 w}{\partial x^3} + H \frac{\partial^3 w}{\partial x \partial y^2} \right), \tag{11}$$

$$\psi_y = \frac{\partial w}{\partial y} + \frac{1}{C_{yz}}\left(D_y \frac{\partial^3 w}{\partial y^3} + H \frac{\partial^3 w}{\partial x^2 \partial y} \right), \tag{12}$$

in which

$$H = D_1 + 2D_{xy}. \tag{13}$$

Then, by substituting Equation (11) and Equation (12) into the strain-displacement and constitutive relationships which have been given by Equation (2) and Equation (4), we can obtain

$$M_x = D_x\left[\frac{\partial^2 w}{\partial x^2} + \frac{1}{C_{xz}}\left(D_x \frac{\partial^4 w}{\partial x^4} + H \frac{\partial^4 w}{\partial x^2 \partial y^2} \right) \right] + D_1\left[\frac{\partial^2 w}{\partial y^2} + \frac{1}{C_{yz}}\left(D_y \frac{\partial^4 w}{\partial y^4} + H \frac{\partial^4 w}{\partial x^2 \partial y^2} \right) \right], \tag{14a}$$

$$M_y = D_1\left[\frac{\partial^2 w}{\partial x^2} + \frac{1}{C_{xz}}\left(D_x \frac{\partial^4 w}{\partial x^4} + H \frac{\partial^4 w}{\partial x^2 \partial y^2} \right) \right] + D_y\left[\frac{\partial^2 w}{\partial y^2} + \frac{1}{C_{yz}}\left(D_y \frac{\partial^4 w}{\partial y^4} + H \frac{\partial^4 w}{\partial x^2 \partial y^2} \right) \right], \tag{14b}$$

$$M_{xy} = D_{xy}\left[2\frac{\partial^2 w}{\partial x \partial y} + \frac{1}{C_{xz}}\left(D_x \frac{\partial^4 w}{\partial x^3 \partial y} + H \frac{\partial^4 w}{\partial x \partial y^3} \right) + \frac{1}{C_{yz}}\left(D_y \frac{\partial^4 w}{\partial x \partial y^3} + H \frac{\partial^4 w}{\partial x^3 \partial y} \right) \right], \tag{14c}$$

$$Q_x = C_{xz}\gamma_x = -\left(D_x\frac{\partial^3 w}{\partial x^3} + H\frac{\partial^3 w}{\partial x \partial y^2}\right), \tag{14d}$$

$$Q_y = C_{yz}\gamma_y = -\left(D_y\frac{\partial^3 w}{\partial y^3} + H\frac{\partial^3 w}{\partial x^2 \partial y}\right). \tag{14e}$$

Next, by substituting above Equations (14a) to (14e) back into Equation (10), the three equilibrium equations of the Mindlin-Reissner plate theory can also be expressed in terms of the deflection w, as follows:

$$\frac{D_x^2}{C_{xz}}\frac{\partial^5 w}{\partial x^5} + \left(\frac{D_x H}{C_{xz}} + \frac{D_1 H}{C_{yz}} + \frac{D_x D_{xy}}{C_{xz}} + \frac{D_{xy} H}{C_{yz}}\right)\frac{\partial^5 w}{\partial x^3 \partial y^2} + \left(\frac{D_1 D_y}{C_{yz}} + \frac{D_{xy} H}{C_{xz}} + \frac{D_{xy} D_y}{C_{yz}}\right)\frac{\partial^5 w}{\partial x \partial y^4} = 0, \tag{15}$$

$$\frac{D_y^2}{C_{yz}}\frac{\partial^5 w}{\partial y^5} + \left(\frac{D_y H}{C_{yz}} + \frac{D_{xy} H}{C_{xz}} + \frac{D_{xy} D_y}{C_{yz}} + \frac{D_1 H}{C_{xz}}\right)\frac{\partial^5 w}{\partial x^2 \partial y^3} + \left(\frac{D_{xy} D_x}{C_{xz}} + \frac{D_{xy} H}{C_{yz}} + \frac{D_1 D_x}{C_{xz}}\right)\frac{\partial^5 w}{\partial x^4 \partial y} = 0, \tag{16}$$

$$D_x\frac{\partial^4 w}{\partial x^4} + 2H\frac{\partial^4 w}{\partial x^2 \partial y^2} + D_y\frac{\partial^4 w}{\partial y^4} = q. \tag{17}$$

Note that it's very difficult and even impossible to simultaneously solve above three equations. Considering that Equation (15) and Equation (16) are much more complicated, we will first solve Equation (17). The solution of Equation (17) can be divided into two parts, i.e., the homogeneous part w^0 and the particular part w^*, which should respectively satisfy

$$D_x\frac{\partial^4 w^0}{\partial x^4} + 2H\frac{\partial^4 w^0}{\partial x^2 \partial y^2} + D_y\frac{\partial^4 w^0}{\partial y^4} = 0, \tag{18}$$

and

$$D_x\frac{\partial^4 w^*}{\partial x^4} + 2H\frac{\partial^4 w^*}{\partial x^2 \partial y^2} + D_y\frac{\partial^4 w^*}{\partial y^4} = q. \tag{19}$$

For the homogeneous part, fourteen linearly independent polynomial solutions are summarized in Table 1, together with their deduced rotation and strain solutions. Besides, when the plate is subjected to a uniformly distributed transverse load q, the particular solution can be simply set as

$$w^* = \frac{q}{48}\left(\frac{x^4}{D_x} + \frac{y^4}{D_y}\right), \tag{20}$$

and accordingly

$$\psi_x^* = \frac{qx^3}{12D_x} + \frac{qx}{2C_{xz}}, \tag{21}$$

$$\psi_y^* = \frac{qy^3}{12D_y} + \frac{qy}{2C_{yz}}. \tag{22}$$

Then substitutions of Equations (20) to (22) back into Equation (2) yields

$$\kappa_x^* = \frac{qx^2}{4D_x} + \frac{q}{2C_{xz}}, \ \kappa_y^* = \frac{qy^2}{4D_y} + \frac{q}{2C_{yz}}, \ \kappa_{xy}^* = 0, \ \gamma_x^* = -\frac{qx}{2C_{xz}}, \ \gamma_y^* = -\frac{qy}{2C_{yz}}. \tag{23}$$

It can be easily proven that, the polynomial functions proposed in Table 1 and Equation (20), whose orders are no greater than four, can also satisfy Equation (15) and Equation (16) which are fifth-order differential equations. That means, these provided homogeneous and particular solutions are exactly the analytical solutions of the orthotropic Mindlin-Reissner plate, and can be employed for constructing finite elements.

3. Finite Element Implementation

3.1 Variational principle

As previously discussed, a straightforward displacement-based finite element implementation using Trefftz solutions will produce non-conforming models. Generally, the sub-region potential energy principle should be employed to ensure the non-conforming elements' convergence properties [45]:

$$\Pi_{mP}^e = \Pi_P^e + H_{ic} , \tag{24}$$

in which Π_P^e is the conventional potential energy functional

$$\Pi_P^e = \iint_\Omega \frac{1}{2} \mathbf{\varepsilon}^\mathrm{T} \mathbf{D} \mathbf{\varepsilon} \mathrm{d}\Omega - \iint_\Omega \mathbf{f}^\mathrm{T} \mathbf{u} \mathrm{d}\Omega - \int_{\Gamma_\sigma} \mathbf{R}^\mathrm{T} \mathbf{u} \mathrm{d}\Gamma , \tag{25}$$

where $\mathbf{f}$ and $\mathbf{R}$ respectively are the prescribed body and boundary loads; H_{ic} is the additional energy item produced by the incompatibilities along element boundary.

Note that the sub-region potential energy principle is much more complicated than the conventional potential energy principle, which will make the element construction procedure more tedious. For simplicity, we will directly use the conventional potential energy functional instead of the sub-region potential energy functional in this work. However, if the simplified functional is improperly employed, the convergence can not be guaranteed. To overcome this problem, the generalized conforming theory proposed by Long et.al [45], which can effectively make $H_{ic} \to 0$ as the mesh refined, will be introduced. The resulting generalized conforming element belongs to

the non-conforming model in a coarse mesh and will converge into a conforming one with the mesh refinement.

3.2 The new 4-node quadrilateral plate element

Figure 2 illustrates a schematic representation of the new 4-node quadrilateral plate element in which 1~4 are the vertex nodes. A_i and B_i $(i = 1 \sim 4)$ are the Gauss points (the local parametric coordinates are $\xi = \pm 1/\sqrt{3}$) for imposing the generalized conforming condition. The element nodal DOF vector can be expressed as

$$\mathbf{q}^e = \begin{bmatrix} w_1 & \psi_{x1} & \psi_{y1} & w_2 & \psi_{x2} & \psi_{y2} & w_3 & \psi_{x3} & \psi_{y3} & w_4 & \psi_{x4} & \psi_{y4} \end{bmatrix}^{\mathrm{T}}. \tag{26}$$

As previously discussed, this new displacement-based plate element will be constructed based on the analytical solutions of the orthotropic Mindlin-Reissner plate. Firstly, the deflection and rotation fields are assumed as

$$\mathbf{u} = \begin{Bmatrix} w \\ \psi_x \\ \psi_y \end{Bmatrix} = \mathbf{U}\boldsymbol{\alpha} + \mathbf{u}^*, \tag{27}$$

with

$$\mathbf{U} = \begin{bmatrix} w^0_1 & w^0_2 & w^0_3 & \cdots & w^0_{12} \\ \psi^0_{x1} & \psi^0_{x2} & \psi^0_{x3} & \cdots & \psi^0_{x12} \\ \psi^0_{y1} & \psi^0_{y2} & \psi^0_{y3} & \cdots & \psi^0_{y12} \end{bmatrix}, \tag{28}$$

$$\boldsymbol{\alpha} = \begin{bmatrix} \alpha_1 & \alpha_2 & \cdots & \alpha_{12} \end{bmatrix}. \tag{29}$$

Accordingly, the bending curvatures and shear strains can be expressed as

$$\boldsymbol{\varepsilon} = \begin{Bmatrix} \kappa_x \\ \kappa_y \\ \kappa_{xy} \\ \gamma_x \\ \gamma_y \end{Bmatrix} = \mathbf{E}\boldsymbol{\alpha} + \boldsymbol{\varepsilon}^*, \tag{30}$$

with

$$\mathbf{E} = \begin{bmatrix} \kappa_{x1}^0 & \kappa_{x2}^0 & \kappa_{x3}^0 & \cdots & \kappa_{x12}^0 \\ \kappa_{y1}^0 & \kappa_{y2}^0 & \kappa_{y3}^0 & \cdots & \kappa_{y12}^0 \\ \kappa_{xy1}^0 & \kappa_{xy2}^0 & \kappa_{xy3}^0 & \cdots & \kappa_{xy12}^0 \\ \gamma_{x1}^0 & \gamma_{x2}^0 & \gamma_{x3}^0 & \cdots & \gamma_{x12}^0 \\ \gamma_{y1}^0 & \gamma_{y2}^0 & \gamma_{y3}^0 & \cdots & \gamma_{y12}^0 \end{bmatrix}. \tag{31}$$

In above equations, the components of the matrices $\mathbf{U}$ and $\mathbf{E}$ are the first twelve groups of homogeneous solutions proposed in Table 1. $\mathbf{u}^*$ and $\boldsymbol{\varepsilon}^*$ correspond to the particular parts and can be calculated by using Equations (20) to (23) for an element-wise constant load q.

Then, in order to determine the introduced unknown coefficients $\alpha_i, (i = 1 \sim 12)$ as shown in Equation (29), the following twelve generalized conforming conditions will be imposed:

(i)   the compatibility conditions for deflections at the four nodes

$$w(x_i, y_i) = w_i, \quad (i = 1 \sim 4), \tag{32}$$

in which $w(x_i, y_i)$ is calculated by using Equation (27) while w_i is the element nodal deflection DOF shown in Equation (26);

(ii)   the compatibility conditions for normal rotations at the Gauss points along each edge

$$\psi_n(x_k, y_k) = \bar{\psi}_{nk}, \quad (k = A_1, B_1, A_2, B_2, A_3, B_3, A_4, B_4), \tag{33}$$

in which $\psi_n(x_k, y_k)$ are also calculated by substituting the Cartesian coordinates into the assumed rotation field shown in Equation (27), while $\bar{\psi}_{nk}$ is interpolated by

$$\bar{\psi}_{nij} = (1 - s)\bar{\psi}_{ni} + s\bar{\psi}_{nj}, \quad s = (\xi + 1)/2, \tag{34}$$

where $\bar{\psi}_{ni}$ and $\bar{\psi}_{nj}$ are the nodal normal rotations along the element edge ij.

It has been demonstrated in [45] that, for a 4-node quadrilateral plate element, above twelve generalized conforming conditions can effectively ensure $H_{ic} \rightarrow 0$ as the mesh refined. That means, the new element's convergence can be guaranteed.

Next, by substituting Equation (27) into Equations (32) and (33), the relations between $\boldsymbol{\alpha}$ and the element nodal DOF vector $\mathbf{q}^e$ are derived:

$$\boldsymbol{\lambda}\boldsymbol{\alpha} + \boldsymbol{\chi} = \boldsymbol{\Lambda}\mathbf{q}^e. \tag{35}$$

For brevity, the detailed expressions of the matrices $\boldsymbol{\lambda}$, $\boldsymbol{\chi}$ and $\boldsymbol{\Lambda}$ will be summarized in

Appendix. From Equation (35), we can obtain

$$\boldsymbol{\alpha} = \mathbf{L}_{\Lambda}\mathbf{q}^{e} - \mathbf{L}_{\chi}, \tag{36}$$

with

$$\mathbf{L}_{\Lambda} = \boldsymbol{\lambda}^{-1}\boldsymbol{\Lambda}, \quad \mathbf{L}_{\chi} = \boldsymbol{\lambda}^{-1}\boldsymbol{\chi}. \tag{37}$$

Substitution of Equation (36) back into Equation (27) and Equation (30) yields

$$\mathbf{u} = \mathbf{N}\mathbf{q}^{e} + \mathbf{N}^{*}, \tag{38}$$

$$\boldsymbol{\varepsilon} = \mathbf{B}\mathbf{q}^{e} + \mathbf{B}^{*}, \tag{39}$$

in which

$$\mathbf{N} = \mathbf{U}\mathbf{L}_{\Lambda}, \quad \mathbf{N}^{*} = \mathbf{u}^{*} - \mathbf{U}\mathbf{L}_{\chi}, \tag{40}$$

$$\mathbf{B} = \mathbf{E}\mathbf{L}_{\Lambda}, \quad \mathbf{B}^{*} = \boldsymbol{\varepsilon}^{*} - \mathbf{E}\mathbf{L}_{\chi}. \tag{41}$$

Finally, by substituting Equation (38) and Equation (39) into Equation (25) and applying the principle of minimum potential energy, we can obtain

$$\mathbf{K}\mathbf{q}^{e} = \mathbf{P}, \tag{42}$$

where $\mathbf{K}$ is the element stiffness matrix

$$\mathbf{K} = \iint_{\Omega} \mathbf{B}^{\mathrm{T}}\mathbf{D}\mathbf{B}\mathrm{d}\Omega, \tag{43}$$

and $\mathbf{P}$ is the element nodal equivalent load vector

$$\mathbf{P} = \iint_{\Omega} \mathbf{N}^{\mathrm{T}}\mathbf{f}\mathrm{d}\Omega + \int_{\Gamma_{\sigma}} \mathbf{N}^{\mathrm{T}}\mathbf{R}\mathrm{d}\Gamma - \iint_{\Omega} \mathbf{B}^{\mathrm{T}}\mathbf{D}\mathbf{B}^{*}\mathrm{d}\Omega. \tag{44}$$

Note that the above element stiffness matrix and the element nodal equivalent load vector are obtained in the local coordinate system, which is in general different with the global coordinate system, as shown in Figure 3. Thus they should be transformed back into the global coordinate system:

$$\mathbf{K}_{\text{global}} = \mathbf{Q}\mathbf{K}\mathbf{Q}^{\mathrm{T}}, \tag{45}$$

$$\mathbf{P}_{\text{global}} = \mathbf{P}\mathbf{Q}^{\mathrm{T}}, \tag{46}$$

with

$$\mathbf{Q} = \begin{bmatrix} \mathbf{Q}_\theta & & & \\ & \mathbf{Q}_\theta & & \\ & & \mathbf{Q}_\theta & \\ & & & \mathbf{Q}_\theta \end{bmatrix}, \tag{47}$$

in which

$$\mathbf{Q}_\theta = \begin{bmatrix} 1 & 0 & 0 \\ 0 & \cos\theta & -\sin\theta \\ 0 & \sin\theta & \cos\theta \end{bmatrix}. \tag{48}$$

This new element will be named by GCTP4, to record that it is a 'Generalized Conforming Trefftz Plate element with 4 nodes'. As preceding discussed, it will perform as a non-conforming model on coarse meshes and gradually converge into the conforming one as the mesh is refined.

4. Numerical validation

The proposed new element GCTP4 will be applied to several numerical benchmark tests. The results are then analyzed and discussed. Besides, the data of some existing plate element models, including QHT-11 [40], Abaqus S4 and S4R [46], RDKQ-L20 [47], SQUAD4 [48] and Petrolito's element [38, 39], are also provided for comparison.

4.1 The patch test

As shown in Figure 4, the small patch is divided into five elements. Two different thicknesses (h=0.02 and 0.2) are considered. The material properties are defined as [40]:

$$E_x = 10E_y = 10, \ G_{xy} = 0.5E_y, \ G_{xz} = 0.5E_y, \ G_{yz} = 0.2E_y, \ \mu_{xy} = 0.25. \tag{49}$$

To produce a constant stress state, the following displacement field will be employed:

$$w = 1 + x + y + x^2 + y^2 + xy, \ \psi_x = 1 + 2x + y, \ \psi_y = 1 + 2y + x. \tag{50}$$

The deflections and rotations at the boundary nodes 1~4 which are calculated by using Equation (50) are imposed to the patch as the boundary conditions, whilst the results at the inner nodes 5~8 are monitored and summarized in Table 2. In the thin plate case with h=0.02, this element can deliver exact results. In the thick plate case with h=0.2, there are tiny errors which are mainly caused by the interelement incompatibilities in a coarse distorted mesh. With the refinement of the mesh, these

errors can be effectively eliminated.

4.2 The square plate subjected to uniformly distributed load

Figure 5 depicts a square plate subjected to a uniformly distributed transverse load q. Due to symmetry, only a quarter of the plate is modeled. The material parameters given by Equation (49) are employed and the non-dimensional deflection and bending moment are calculated:

$$\bar{w} = w \times \left(100 E_y h^3 / qL^4\right), \quad \bar{M} = M \times \left(10 / qL^2\right). \tag{51}$$

(a) Convergence

The convergence of the proposed new element will be investigated using the typical mesh shown in Figure 5. Two cases with different boundary conditions, i.e., the clamped case and simply supported case, are considered. Figures 6 to 9 give the relative errors of the central deflections and moments for two different thickness-span ratios (h/L=0.01, 0.1), in which the reference values are provided in [40]. One can see that the new element GCTP4 convergences very rapidly. An interesting feature is that this new displacement-based element can also provide quite good performance when predicting stress resultants.

(b) Sensitivity to mesh distortion

To assess the element's sensitivity to mesh distortion, the clamped square plate is analyzed again. As shown in Figure 10, two different distorted meshes containing only 2×2 elements are employed. In the first one, the central node is moved along the main diagonal of the plate to the corner node. In the second one, the central node is vertically moved to the symmetry edge. Figure 11 illustrates the variation of the normalized central deflection versus the distortion parameter. It can be observed that the maximum deviation is no larger than 5%, revealing that the element has good resistances to mesh distortion.

4.3 The two-span plate

As shown in Figure 12, this test involves a two-span plate which is simply supported along the *y*-direction at its left, right and middle edges. The left-span of the plate is subjected to a distributed transverse load q, while the right-span is without loading. Two cases with different thickness-span

ratios h/L=0.01 and 0.1 are considered. The material parameters used here are the same with the previous test.

First, the convergence will be investigated. The computations are repeatedly carried out by using the mesh 2N×N with N=2, 4, 8, 16. In Figures 13 and 14, the relative errors of the deflection and bending moment calculated at the point A are proposed. Second, the coarse mesh 4×2 is employed to generate distorted meshes, as shown in Figure 15, to further study the influences on element performance of mesh distortion. Figure 16 gives the variation of the deflection versus the distortion parameter. The results of this test reveal once again that this new element GCTP4 has good numerical accuracy and low susceptibility to mesh distortion.

4.4 The rectangular plate with different sizes

In this test, the rectangular plates with different length a, width b and thickness h are analyzed to evaluate the rationalities of the present element formulation. The material parameters proposed in [49] are adopted here:

$$E_x = 20.83, \ E_y = 10.94, \ G_{xy} = 6.10, \ G_{xz} = 3.71, G_{yz} = 6.19, \mu_{xy} = 0.44 , \tag{52}$$

and the non-dimensional deflection are checked:

$$\bar{w} = wQ_{11}/hq , \ Q_{11} = E_x \big/ \left(1 - \mu_{xy}\mu_{yx}\right). \tag{53}$$

In Table 3 the numerical results calculated by using a refined mesh 32×32 are summarized. Besides, the reference values which are obtained using the series expansion method based on different plate theories, including the high order shear deformation plate theory [49], the classical thin plate theory [50], the first order shear deformation plate theory [50], the two-variable refined plate theory [50] and the 3D elastic theory [51], are also listed. It seems that the results of the high order shear deformation theory [49] are more close to the new plate element.

4.5 The circular plate subjected to uniformly distributed load

In this test, the clamped circular plate is subjected to a uniformly distributed load. As shown in Figure 17, only a quarter of the plate is analyzed due to symmetry. The material parameters are described as [40]

$$E_x = 5.6, \ E_y = 1.2, \ G_{xy} = G_{xz} = G_{yz} = 0.6, \mu_{xy} = 0.26 . \tag{54}$$

Then the non-dimensional central deflection is calculated:

$$\bar{w} = wD/qR^4 \ , \ D = 3\left(D_x + D_y\right) + 2H \ . \tag{55}$$

In Table 4, the results for three different thickness-radius ratio cases (h/R=0.001, 0.01 and 0.1) are summarized. It can be seen that this new element has good numerical accuracy and is free of shear locking.

5. Conclusions

This work proposes a simple but robust 4-node 12-DOF quadrilateral displacement-based Trefftz plate element for efficiently analysis of orthotropic plate structures. This is achieved via two main steps. First, the Trefftz functions of the orthotropic Mindlin-Reissner plate are derived and employed for formulating the element's deflection and rotation fields. Second, to guarantee the convergence property and future enrich the element behaviors, the generalized conforming conditions are employed to satisfy the requirements for interelement compatibility in weak sense. The resulting displacement-based Trefftz plate element, named as GCTP4, has the following characteristics:

(i) Since the element is developed based on the generalized conforming theory, it will behave as a non-conforming model on coarse meshes and gradually converge into a conforming model with the mesh refinement.

(ii) Numerical tests reveal that the new element can produce high precision results for both the displacement and stress resultant in analysis of thick and thin plates. Moreover, it is free of shear locking and has good robustness to mesh distortion.

(iii) Compared with its hybrid/mixed counterparts, the displacement-based Trefftz plate element can be extended to the geometric nonlinear cases more directly. Related topics will be discussed in our future papers.

Appendix

In this section, the components of the matrices $\boldsymbol{\lambda}$, $\boldsymbol{\chi}$ and $\boldsymbol{\Lambda}$ shown in Equation (35) are presented in details. Firstly, the matrix $\boldsymbol{\lambda}$ can be obtained by

$$\boldsymbol{\lambda} = \begin{bmatrix} \boldsymbol{\lambda}^w \\ \boldsymbol{\lambda}^\phi \end{bmatrix}, \tag{A1}$$

in which

$$\boldsymbol{\lambda}^w = \begin{bmatrix} w^0_1(x_1, y_1) & w^0_2(x_1, y_1) & w^0_3(x_1, y_1) & \cdots & w^0_{12}(x_1, y_1) \\ w^0_1(x_2, y_2) & w^0_2(x_2, y_2) & w^0_3(x_2, y_2) & \cdots & w^0_{12}(x_2, y_2) \\ w^0_1(x_3, y_3) & w^0_2(x_3, y_3) & w^0_3(x_3, y_3) & \cdots & w^0_{12}(x_3, y_3) \\ w^0_1(x_4, y_4) & w^0_2(x_4, y_4) & w^0_3(x_4, y_4) & \cdots & w^0_{12}(x_4, y_4) \end{bmatrix}, \tag{A2}$$

$$\boldsymbol{\lambda}^\phi = \mathbf{T}_n \boldsymbol{\Phi}, \tag{A3}$$

with

$$\boldsymbol{\Phi} = \begin{bmatrix} \psi^0_{x1}(x_{A1}, y_{A1}) & \psi^0_{x2}(x_{A1}, y_{A1}) & \cdots & \psi^0_{x12}(x_{A1}, y_{A1}) \\ \psi^0_{y1}(x_{A1}, y_{A1}) & \psi^0_{y2}(x_{A1}, y_{A1}) & \cdots & \psi^0_{y12}(x_{A1}, y_{A1}) \\ \vdots & \vdots & \ddots & \vdots \\ \psi^0_{x1}(x_{B4}, y_{B4}) & \psi^0_{x2}(x_{B4}, y_{B4}) & \cdots & \psi^0_{x12}(x_{B4}, y_{B4}) \\ \psi^0_{y1}(x_{B4}, y_{B4}) & \psi^0_{y2}(x_{B4}, y_{B4}) & \cdots & \psi^0_{y12}(x_{B4}, y_{B4}) \end{bmatrix}, \tag{A4}$$

$$\mathbf{T}_n = \begin{bmatrix} \mathbf{T}_1 & & & \\ & \mathbf{T}_2 & & \\ & & \mathbf{T}_3 & \\ & & & \mathbf{T}_4 \end{bmatrix}, \quad \mathbf{T}_i = \begin{bmatrix} l_{ij} & m_{ij} & & \\ & & l_{ij} & m_{ij} \end{bmatrix}, \quad (ij = 12, 23, 34, 41), \tag{A5}$$

where l_{ij} and m_{ij} denote the direction cosines of the outer normal of the element edge ij.

Secondly, the matrix $\boldsymbol{\chi}$ is obtained by

$$\boldsymbol{\chi} = \begin{bmatrix} \boldsymbol{\chi}^w \\ \boldsymbol{\chi}^\phi \end{bmatrix}, \tag{A6}$$

in which

$$\boldsymbol{\chi}^w = \begin{bmatrix} w^*(x_1, y_1) \\ w^*(x_2, y_2) \\ w^*(x_3, y_3) \\ w^*(x_4, y_4) \end{bmatrix}, \tag{A7}$$

$$\boldsymbol{\chi}^\phi = \mathbf{T}_n \boldsymbol{\Phi}^*, \tag{A8}$$

with

$$\mathbf{\Phi}^* = \begin{bmatrix} \psi_x^*(x_{A1}, y_{A1}) \\ \psi_y^*(x_{A1}, y_{A1}) \\ \vdots \\ \psi_x^*(x_{B4}, y_{B4}) \\ \psi_y^*(x_{B4}, y_{B4}) \end{bmatrix}. \tag{A9}$$

Finally, the matrix $\mathbf{\Lambda}$ is given by

$$\mathbf{\Lambda} = \begin{bmatrix} \mathbf{\Lambda}^w \\ \mathbf{\Lambda}^\phi \end{bmatrix}, \tag{A10}$$

in which

$$\mathbf{\Lambda}^w = \begin{bmatrix} \mathbf{I}_{1\times 3} & & & \\ & \mathbf{I}_{1\times 3} & & \\ & & \mathbf{I}_{1\times 3} & \\ & & & \mathbf{I}_{1\times 3} \end{bmatrix}, \quad \mathbf{I}_{1\times 3} = \begin{bmatrix} 1 & 0 & 0 \end{bmatrix}, \tag{A11}$$

$$\mathbf{\Lambda}^\phi = \begin{bmatrix} \mathbf{\Lambda}_{11}^\phi & \mathbf{\Lambda}_{12}^\phi & & \\ & \mathbf{\Lambda}_{22}^\phi & \mathbf{\Lambda}_{23}^\phi & \\ & & \mathbf{\Lambda}_{33}^\phi & \mathbf{\Lambda}_{34}^\phi \\ \mathbf{\Lambda}_{41}^\phi & & & \mathbf{\Lambda}_{44}^\phi \end{bmatrix}, \tag{A12}$$

with

$$\mathbf{\Lambda}_{11}^\phi = \begin{bmatrix} 0 & -\dfrac{1}{l_{12}}(1-s_{A1})y_{12} & \dfrac{1}{l_{12}}(1-s_{A1})x_{12} \\ 0 & -\dfrac{1}{l_{12}}(1-s_{B1})y_{12} & \dfrac{1}{l_{12}}(1-s_{B1})x_{12} \end{bmatrix}, \quad \mathbf{\Lambda}_{12}^\phi = \begin{bmatrix} 0 & -\dfrac{1}{l_{12}}s_{A1}y_{12} & \dfrac{1}{l_{12}}s_{A1}x_{12} \\ 0 & -\dfrac{1}{l_{12}}s_{B1}y_{12} & \dfrac{1}{l_{12}}s_{B1}x_{12} \end{bmatrix}, \tag{A13a}$$

$$\mathbf{\Lambda}_{22}^\phi = \begin{bmatrix} 0 & -\dfrac{1}{l_{23}}(1-s_{A2})y_{23} & \dfrac{1}{l_{23}}(1-s_{A2})x_{23} \\ 0 & -\dfrac{1}{l_{23}}(1-s_{B2})y_{23} & \dfrac{1}{l_{23}}(1-s_{B2})x_{23} \end{bmatrix}, \quad \mathbf{\Lambda}_{23}^\phi = \begin{bmatrix} 0 & -\dfrac{1}{l_{23}}s_{A2}y_{23} & \dfrac{1}{l_{23}}s_{A2}x_{23} \\ 0 & -\dfrac{1}{l_{23}}s_{B2}y_{23} & \dfrac{1}{l_{23}}s_{B2}x_{23} \end{bmatrix}, \tag{A13b}$$

$$\mathbf{\Lambda}_{33}^\phi = \begin{bmatrix} 0 & -\dfrac{1}{l_{34}}(1-s_{A3})y_{34} & \dfrac{1}{l_{34}}(1-s_{A3})x_{34} \\ 0 & -\dfrac{1}{l_{34}}(1-s_{B3})y_{34} & \dfrac{1}{l_{34}}(1-s_{B3})x_{34} \end{bmatrix}, \quad \mathbf{\Lambda}_{34}^\phi = \begin{bmatrix} 0 & -\dfrac{1}{l_{34}}s_{A3}y_{34} & \dfrac{1}{l_{34}}s_{A3}x_{34} \\ 0 & -\dfrac{1}{l_{34}}s_{B3}y_{34} & \dfrac{1}{l_{34}}s_{B3}x_{34} \end{bmatrix}, \tag{A13c}$$

$$\mathbf{\Lambda}_{44}^\phi = \begin{bmatrix} 0 & -\dfrac{1}{l_{41}}(1-s_{A4})y_{41} & \dfrac{1}{l_{41}}(1-s_{A4})x_{41} \\ 0 & -\dfrac{1}{l_{41}}(1-s_{A4})y_{41} & \dfrac{1}{l_{41}}(1-s_{A4})x_{41} \end{bmatrix}, \quad \mathbf{\Lambda}_{41}^\phi = \begin{bmatrix} 0 & -\dfrac{1}{l_{41}}s_{A4}y_{41} & \dfrac{1}{l_{41}}s_{A4}x_{41} \\ 0 & -\dfrac{1}{l_{41}}s_{B4}y_{41} & \dfrac{1}{l_{41}}s_{B4}x_{41} \end{bmatrix}. \tag{A13d}$$

Acknowledgements

Reference

[1] Hrabok MM, Hrudey TM|. A review and catalogue of plate bending finite elements. Computers & Structures 1984; 19(3): 479-795.

[2] Reddy JN. A simple higher-order theory for laminated composite plates. Journal of Applied Mechanics 1984; 51(4): 745-752.

[3] Ahmed A, Kapuria S. A four-node facet shell element for laminated shells based on the third order zigzag theory. Composite Structures 2016; 158: 112-127.

[4] Eijo A, Onate E, Oller S. A four-noded quadrilateral element for composite laminated plates/shells using the refined zigzag theory. International Journal for Numerical Methods in Engineering 2013; 95(8): 631-660.

[5] Iurlaro L, Gherlone M, Di Sciuva M, Tessler A. Refined zigzag theory for laminated composite and sandwich plates derived from Reissner's mixed variational theorem. Composite Structures 2015; 133: 809-817.

[6] Li Q, Liu Y, Zhang Z, Zhong W. A new reduced integration solid-shell element based on EAS and ANS with hourglass stabilization. International Journal for Numerical Methods in Engineering 2015; 104(8): 805-826.

[7] Vu-Quoc L, Tan XG. Efficient hybrid-EAS solid element for accurate stress prediction in thick laminated beams, plates, and shells. Computer Methods in Applied Mechanics and Engineering 2013; 253: 337-355.

[8] Li ZX, Vu-Quoc L. An efficient co-rotational formulation for curved triangular shell element. International Journal for Numerical Methods in Engineering 2007; 72(9): 1029-1062.

[9] Vu-Quoc L, Tan XG. Optimal solid shells for non-linear analyses of multilayer composites. I. Statics. Computer Methods in Applied Mechanics and Engineering 2003; 192(9): 975-1016.

[10] Choi JH, Lee BC. Rotation-free triangular shell element using node-based smoothed finite element method. International Journal for Numerical Methods in Engineering 2018; 116(6): 359-379.

[11] Wan D, Hu D, Natarajan S, Bordas SPA, Long T. A linear smoothed quadratic finite element for the analysis of laminated composite Reissner-Mindlin plates. Composite Structures 2017; 180: 395-411.

[12] Zeng W, Liu GR. Smoothed finite element methods (S-FEM): An overview and recent developments. Archives of Computational Methods in Engineering 2016: 1-39.

[13] Nguyen-Thoi T, Phung-Van P, Luong-Van H, Nguyen-Van H, Nguyen-Xuan H. A cell-based smoothed three-node Mindlin plate element (CS-MIN3) for static and free vibration analyses of

plates. Computational Mechanics 2013; 51(1): 65-81.

[14] Nguyen-Xuan H, Rabczuk T, Nguyen-Thanh N, Nguyen-Thoi T, Bordas S. A node-based smoothed finite element method with stabilized discrete shear gap technique for analysis of Reissner-Mindlin plates. Computational mechanics 2010; 46(5): 679-701.

[15] Luong-Van H, Nguyen-Thoi T, Liu GR, Phung-Van P. A cell-based smoothed finite element method using Mindlin plate element (CS-FEM-MIN3) for dynamic response of composite plates on viscoelastic foundation. Engineering Analysis with Boundary Elements 2014; 42: 8-19.

[16] Wang Y, Shi GY, Wang XD. Displacement and stress analysis of laminated composite plates using an eight-node quasi-conforming solid-shell element. Curved & Layered Structures 2017; 4(1): 8-20.

[17] Wang CS, Wang X, Zhang XK, Hu P. Assumed stress quasi-conforming technique for static and free vibration analysis of Reissner-Mindlin plates. International Journal for Numerical Methods in Engineering 2017; 112(4): 303-337.

[18] Hu P, Xia Y, Tang LM. A four-node Reissner-Mindlin shell with assumed displacement quasi-conforming method. CMES-Computer Modeling in Engineering & Sciences 2011; 73(2):103-135.

[19] Bathe KJ, Brezzi F, Cho SW. The MITC7 and MITC9 plate bending elements. Computers & Structures 1989; 32(3-4): 797-814.

[20] Ko Y, Lee Y, Lee PS, Bathe KJ. Performance of the MITC3+ and MITC4+ shell elements in widely-used benchmark problems. Computers & Structures 2017; 193: 187-206.

[21] Katili I, Maknun IJ, Batoz JL, Katili AM. Asymptotic equivalence of DKMT and MITC3 elements for thick composite plates. Composite Structures 2018; 206: 363-379.

[22] Wu Z, Ma R, Chen WJ. A refined three-node triangular element based on the HW variational theorem for multilayered composite plates. Composite Structures 2017; 161: 132-144.

[23] Chen WJ, Cheung YK. Refined discrete quadrilateral degenerated shell element by using Timoshenko's beam function. International Journal for Numerical Methods in Engineering 2005; 63(8): 1203-1227.

[24] Ribaric D, Jelenic G. Higher-order linked interpolation in quadrilateral thick plate finite elements. Finite Elements in Analysis and Design 2012; 51: 67-80.

[25] Ribaric D, Jelenic G. Distortion-immune nine-node displacement-based quadrilateral thick plate finite elements that satisfy constant-bending patch test. International Journal for Numerical Methods in Engineering 2014; 98(7): 492-517.

[26] Cen S, Shang Y. Developments of Mindlin-Reissner Plate Elements. Mathematical Problems in Engineering 2015; 501: 456740.

[27] Jirousek J, Leon N. A powerful finite element for plate bending. Computer Methods in Applied Mechanics and Engineering 1977; 12(1): 77-96.

[28] Jirousek J. Improvement of computational-efficiency of the 9-DOF triangular hybrid-Trefftz plate bending element. International Journal for Numerical Methods in Engineering 1986; 23(11): 2167-2168.

[29] Petrolito J. Hybrid-Trefftz quadrilateral elements for thick plate analysis. Computer Methods in Applied Mechanics and Engineering 1990; 78(3): 331-351.

[30] Kita E, Kamiya N. Trefftz method: an overview. Advances in Engineering Software 1995; 24(1-3): 3-12.

[31] Moldovan ID, Cismaşiu I. FreeHyTE: a hybrid-Trefftz finite element platform. Advances in

Engineering Software 2018; 121: 98-119.

[32] Martins PHC, Bussamra FLS, Lucena Neto E. Three dimensional hybrid-Trefftz stress finite elements for plates and shells. International Journal for Numerical Methods in Engineering 2018; 113(11): 1676-1696.

[33] Moldovan ID. A new approach to non-homogeneous hyperbolic boundary value problems using hybrid-Trefftz stress finite elements. Engineering Analysis with Boundary Elements 2016; 69: 57-71.

[34] Moldovan ID. A new particular solution strategy for hyperbolic boundary value problems using hybrid-Trefftz displacement elements. International Journal for Numerical Methods in Engineering 2015; 102(6): 1293-1315.

[35] Petrolito J. Triangular thick plate elements based on a hybrid-Trefftz approach. Computers & structures 1996; 60(6): 883-894.

[36] Cen S, Shang Y, Li CF, Li HG. Hybrid displacement function element method: a simple hybrid-Trefftz stress element method for analysis of Mindlin-Reissner plate. International Journal for Numerical Methods in Engineering 2014; 98(3): 203-234.

[37] Choo YS, Choi N, Lee BC. Quadrilateral and triangular plane elements with rotational degrees of freedom based on the hybrid Trefftz method. Finite elements in analysis and design 2006; 42(11): 1002-1008.

[38] Petrolito J. Vibration and stability analysis of thick orthotropic plates using hybrid-Trefftz elements. Applied Mathematical Modelling 2014; 38(24): 5858-5869.

[39] Petrolito J. Analysis of orthotropic thick plates using hybrid-Trefftz elements. Proceedings of Australian Conference of the Mechanics of Structures and Materials 2010.

[40] Karkon M, Rezaiee-Pajand M. Hybrid-Trefftz formulation for analysis of thick orthotropic plates. Aerospace Science and Technology 2016; 50: 234-244.

[41] Ray M. A novel hybrid-Trefftz finite element for symmetric laminated composite plates. International Journal of Mechanics and Materials in Design 2018; https://doi.org/10.1007/s10999-018-9422-9.

[42] Li Z, Cen S, Wu CJ, Shang Y, Li CF. High-performance geometric nonlinear analysis with the unsymmetric 4-node, 8-DOF plane element US-ATFQ4. International Journal for Numerical Methods in Engineering 2018; 114(9): 931-954.

[43] Long Y, Xu Y. Generalized conforming triangular membrane element with vertex rigid rotational freedoms. Finite Elements in Analysis and Design 1994; 17(4): 259-271.

[44] Shang Y, Cen S, Li CF, Fu XR. Two generalized conforming quadrilateral Mindlin-Reissner plate elements based on the displacement function. Finite Elements in Analysis and Design 2015; 99: 24-38.

[45] Long YQ, Cen S, Long ZF. Advanced finite element method in structural engineering: Springer, Berlin, 2009.

[46] Abaqus 6.9, HTML Documentation, Dassault Systèmes Simulia Corp, Providence, RI, USA, 2009.

[47] Zhang YX, Kim KS. Two simple and efficient displacement-based quadrilateral elements for the analysis of composite laminated plates. International Journal for Numerical Methods in Engineering 2004; 61(11): 1771-1796.

[48] Wilt TE, Saleeb AF, Chang TY. A mixed element for laminated plates and shells. Computers & Structures 1990; 37(4): 597-611.

[49] Reddy JN. A refined nonlinear theory of plates with transverse shear deformation. International Journal of Solids and Structures 1984; 20(9): 881-896.

[50] Shimpi RP, Patel HG. A two variable refined plate theory for orthotropic plate analysis. International Journal of Solids and Structures 2006; 43(22): 6783-6799.

[51] Srinivas S, Rao A. Bending, vibration and buckling of simply supported thick orthotropic rectangular plates and laminates. International Journal of Solids and Structures 1970; 6(11): 1463-1481.

Table 1. The homogeneous solutions of Equation (18) and the deduced rotations and strains

i	1	2	3	4	5	6	7	8	9	10	11
w^i	1	x	y	x^2	xy	y^2	x^3	x^2y	xy^2	y^3	x^3y
ψ_x^i	0	1	0	$2x$	y	0	$3x^2+\dfrac{6D_x}{C_{xz}}$	$2xy$	$y^2+\dfrac{2H}{C_{xz}}$	0	$3x^2y+\dfrac{6D_x}{C_{xz}}y$
ψ_y^i	0	0	1	0	x	$2y$	0	$x^2+\dfrac{2H}{C_{yz}}$	$2xy$	$3y^2+\dfrac{6D_y}{C_{yz}}$	$x^3+\dfrac{6H}{C_{yz}}x$
κ_x^i	0	0	0	2	0	0	$6x$	$2y$	0	0	$6xy$
κ_y^i	0	0	0	0	0	2	0	0	$2x$	$6y$	0
κ_{xy}^i	0	0	0	0	2	0	0	$4x$	$4y$	0	$6x^2+\dfrac{6D_x}{C_{xz}}+\dfrac{6H}{C_{yz}}$
γ_x^i	0	0	0	0	0	0	$-\dfrac{6D_x}{C_{xz}}$	0	$-\dfrac{2H}{C_{xz}}$	0	$-\dfrac{6D_x}{C_{xz}}y$
γ_y^i	0	0	0	0	0	0	0	$-\dfrac{2H}{C_{yz}}$	0	$-\dfrac{6D_y}{C_{yz}}$	$-\dfrac{6H}{C_{yz}}x$

i	12	13	14
w^i	xy^3	$D_y x^4 - D_x y^4$	$Hx^4 - 3\left(D_x + D_y\right)x^2 y^2 + Hy^4$
ψ_x^i	$y^3 + \dfrac{6H}{C_{xz}}y$	$4D_y x^3 + \dfrac{24D_x D_y}{C_{xz}}x$	$4Hx^3 - 6\left(D_x + D_y\right)xy^2 + \dfrac{12H}{C_{xz}}\left(D_x - D_y\right)x$
ψ_y^i	$3xy^2 + \dfrac{6D_y}{C_{yz}}x$	$-4D_x y^3 - \dfrac{24D_x D_y}{C_{yz}}y$	$4Hy^3 - 6\left(D_x + D_y\right)x^2 y + \dfrac{12H}{C_{yz}}\left(D_y - D_x\right)y$
κ_x^i	0	$12D_y x^2 + \dfrac{24D_x D_y}{C_{xz}}$	$12Hx^2 - 6\left(D_x + D_y\right)y^2 + \dfrac{12H}{C_{xz}}\left(D_x - D_y\right)$
κ_y^i	$6xy$	$-12D_x y^2 - \dfrac{24D_x D_y}{C_{yz}}$	$12Hy^2 - 6\left(D_x + D_y\right)x^2 + \dfrac{12H}{C_{yz}}\left(D_y - D_x\right)$
κ_{xy}^i	$6y^2 + \dfrac{6D_y}{C_{yz}} + \dfrac{6H}{C_{xz}}$	0	$-24\left(D_x + D_y\right)xy$
γ_x^i	$-\dfrac{6H}{C_{xz}}y$	$-\dfrac{24D_x D_y}{C_{xz}}x$	$-\dfrac{12H}{C_{xz}}\left(D_x - D_y\right)x$
γ_y^i	$-\dfrac{6D_y}{C_{yz}}x$	$\dfrac{24D_x D_y}{C_{yz}}y$	$-\dfrac{12H}{C_{yz}}\left(D_y - D_x\right)y$

Table 2. The results of the patch test

Node		h=0.02			h=0.2		
		Exact	GCPT4	Relative Error	Exact	GCPT4	Relative Error
5	w	125	125.00	0%	125	125.06	0.048%
	ψ_x	21	21.00	0%	21	21.00	0.000%
	ψ_y	17	17.00	0%	17	17.00	0.000%
6	w	1291	1291.00	0%	1291	1291.08	0.006%
	ψ_x	71	71.00	0%	71	71.00	0.000%
	ψ_y	45	45.00	0%	45	45.01	0.022%
7	w	1715	1715.00	0%	1715	1715.08	0.005%
	ψ_x	79	79.00	0%	79	78.99	-0.013%
	ψ_y	61	61.00	0%	61	60.99	-0.016%
8	w	707	707.00	0%	707	707.10	0.014%
	ψ_x	47	47.00	0%	47	46.99	-0.021%
	ψ_y	45	45.00	0%	45	45.01	0.022%

Table 3. The dimensionless central deflection of the simply supported rectangular plate with different sizes

b/a	h/a	CPT [50]	RPT [50]	FSDT [50]	HSDT [49]	3D [51]	**GCTP4**
	0.05	21201	21513.5	21542	21542	21542	**21542.9**
2.0	0.1	1325.1	1402.24	1408.4	1408.5	1408.5	**1409.7**
	0.14	344.93	384.20	387.27	387.5	387.23	**387.55**
	0.05	10246	10413.4	10442	10450	10443	**10444.4**
1.0	0.1	640.39	681.73	688.37	689.5	688.57	**689.32**
	0.14	166.7	187.75	191.02	191.6	191.07	**191.57**
	0.05	1988.1	2042.74	2047.9	2051.0	2048.7	**2050.61**
0.5	0.1	124.26	137.82	138.93	139.8	139.08	**139.77**
	0.14	32.345	39.26	39.753	40.21	39.79	**40.21**

Table 4. The dimensionless central deflection of the clamped circular plate

Elements	12	48	192	Reference
h/R=0.001				
RDKQ-L20 [47]	0.1269	0.1259	—	0.1250
SQUAD4 [48]	0.1163	0.1231	0.1246	
QHT-11 [40]	0.1186	0.1234	—	
GCTP4	**0.1194**	**0.1235**	**0.1246**	
h/R=0.01				
RDKQ-L20 [47]	0.1245	0.1251	—	
SQUAD4 [48]	0.1193	0.1242	0.1249	
QHT-11 [40]	0.1187	0.1235	—	
GCTP4	**0.1195**	**0.1236**	**0.1247**	
h/R=0.1				
RDKQ-L20 [47]	0.1244	0.1251	—	
SQUAD4 [48]	0.1355	0.1378	0.1384	
QHT-11 [40]	0.1313	0.1362	—	
GCTP4	**0.1327**	**0.1363**	**0.1379**	
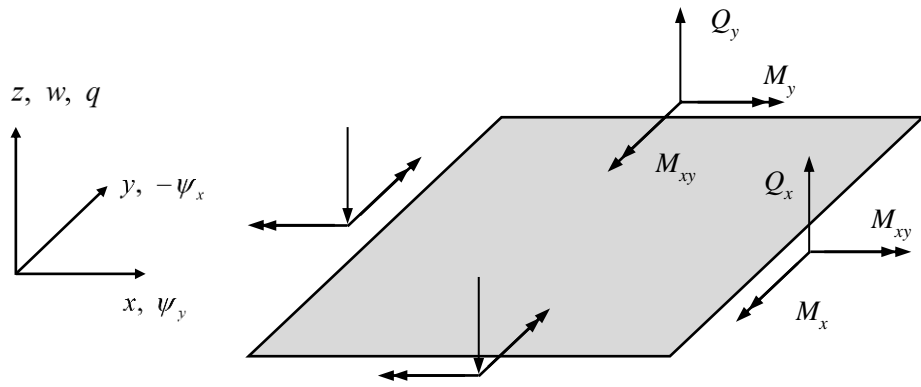
Figure 1. The definitions for a Mindlin-Reissner plate
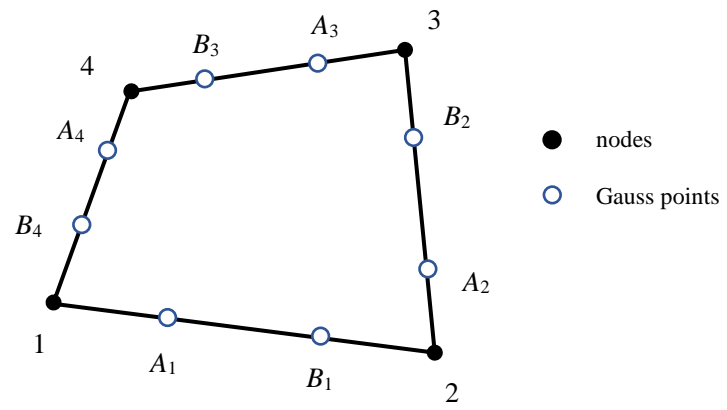
Figure 2. The new 4-node quadrilateral plate element
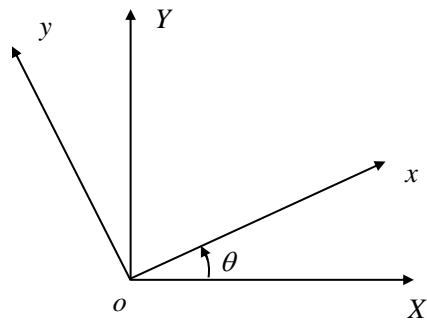
Figure 3. The relationship between the global coordinate system (X, Y)
and the local coordinate system (x, y)

4 (0, 20) 3 (40, 20)

8

7

5: (8, 4)
6: (32, 6)
7: (32, 14)
8: (16, 14)

6

5

1 (0, 0) 2 (40, 0)
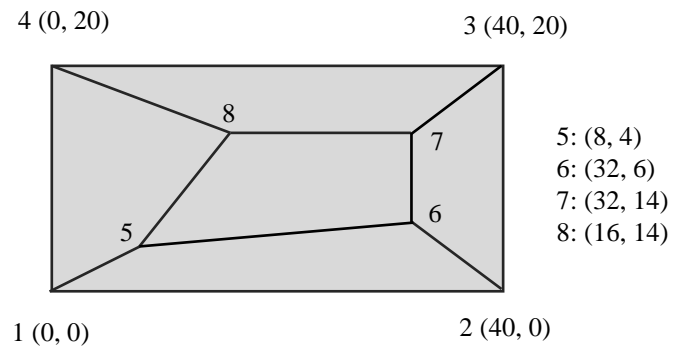
Figure 4. The mesh for the patch test
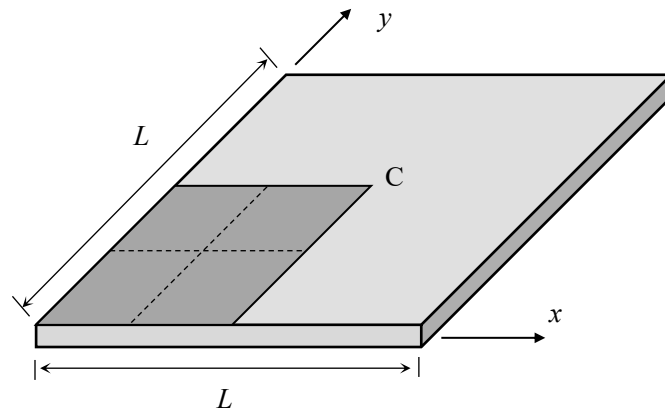
Figure 5. The square plate subjected to a uniformly distributed load
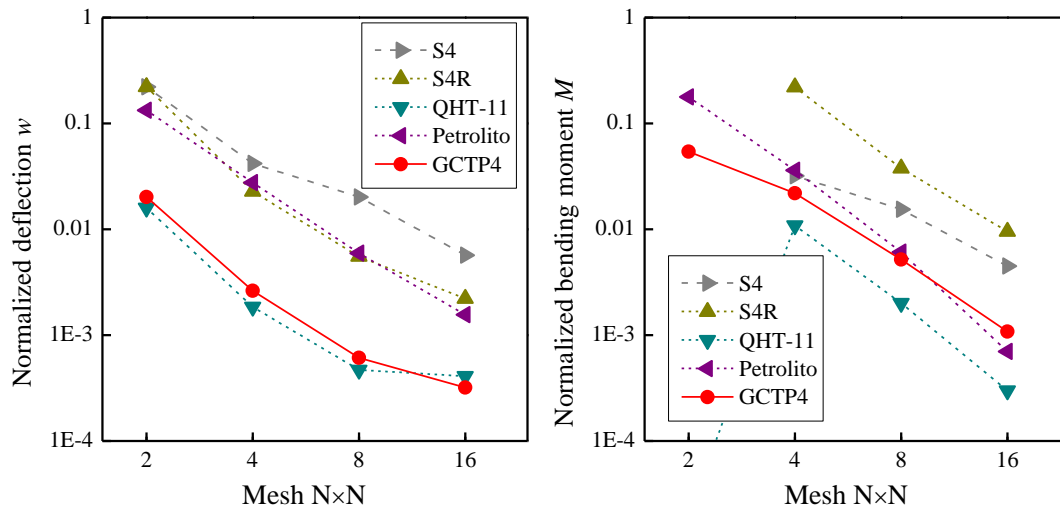
Figure 6. The relative errors of the central deflection and bending moment of the clamped square plate with h/L=0.01
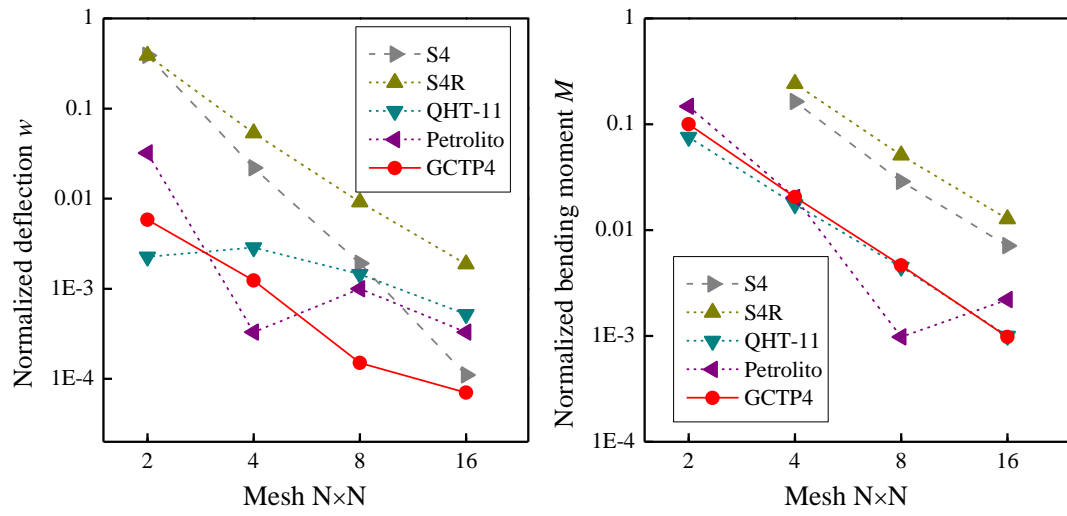
Figure 7. The relative errors of the central deflection and bending moment of the clamped square plate with $h/L=0.1$
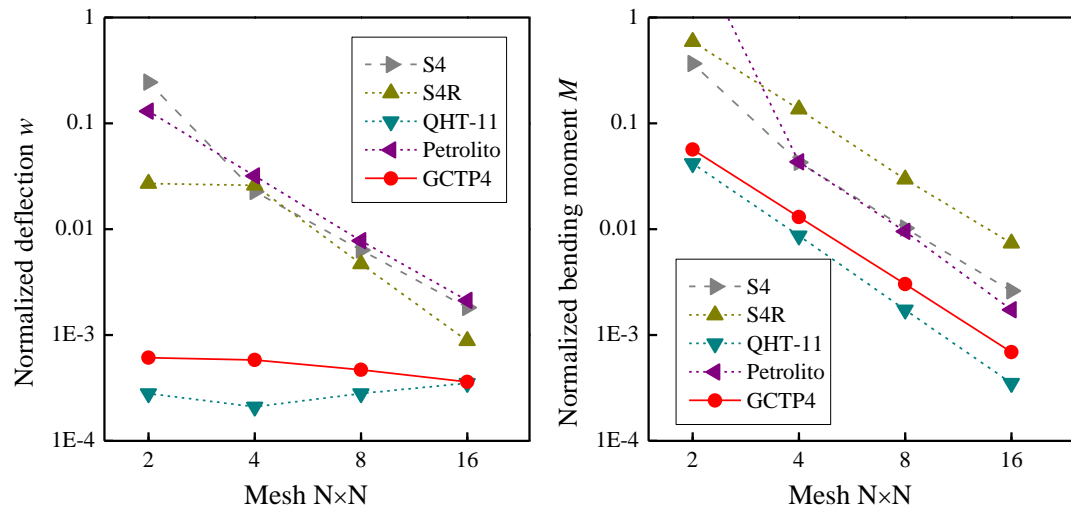
Figure 8. The relative errors of the central deflection and bending moment of the simply supported square plate with h/L=0.01
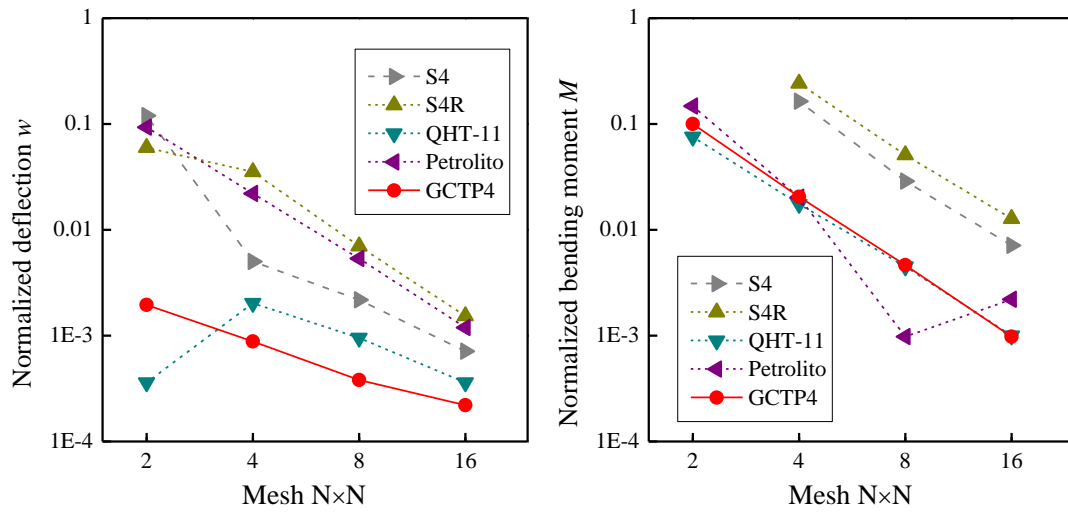
Figure 9. The relative errors of the central deflection and bending moment of the simply supported square plate with h/L=0.1
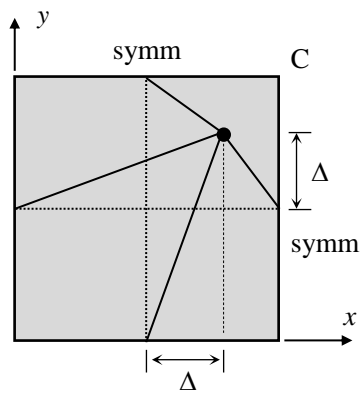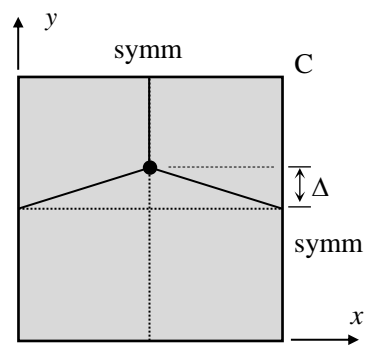
(a)   Distorted mesh A   (b)   Distorted mesh B

Figure 10. Distorted meshes containing 2×2 elements for the clamped square plate
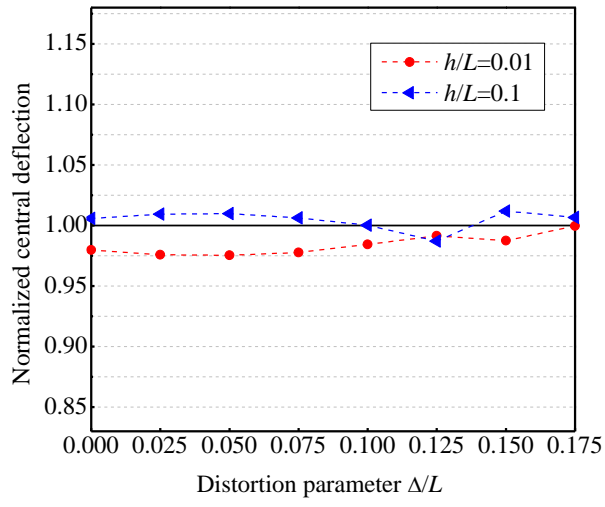
(a) Distorted Mesh A
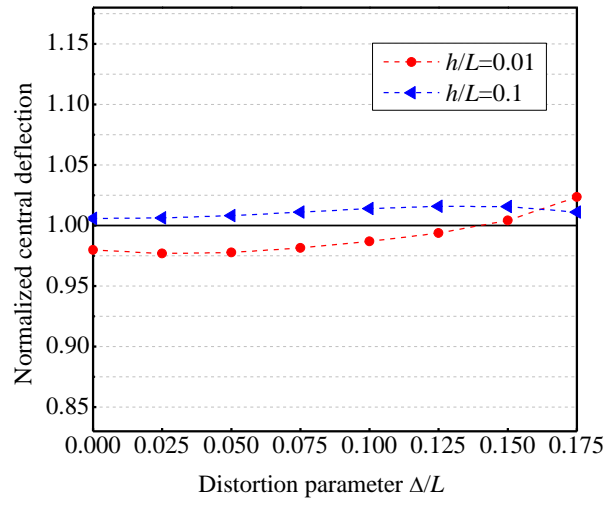
(b) Distorted Mesh B

Figure 11. The normalized central deflection of the clamped plate versus the distortion parameter
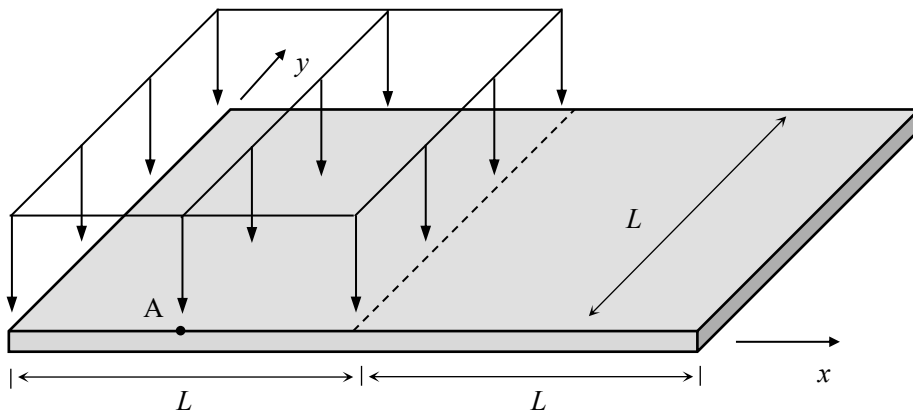
Figure 12. The two-span rectangular plate
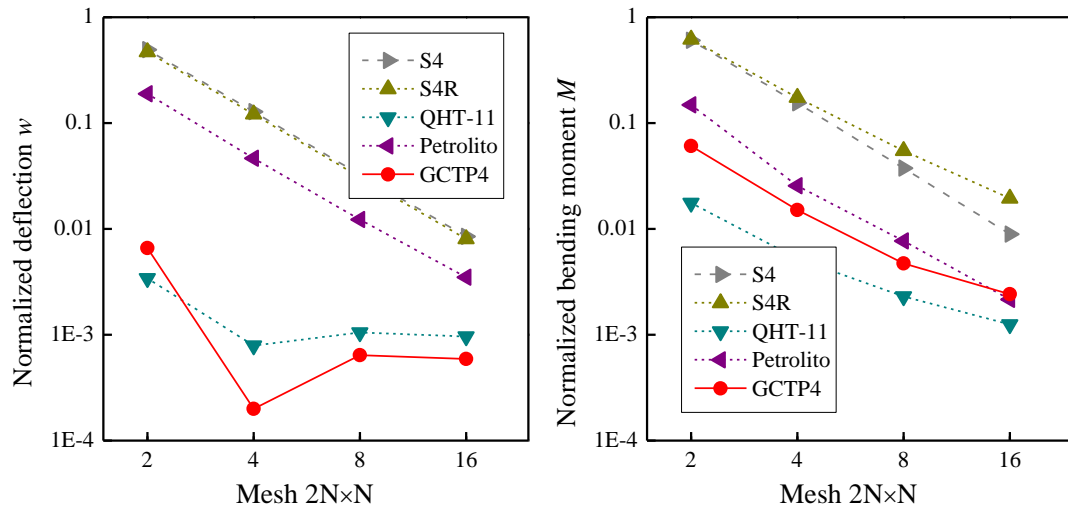
Figure 13. The relative errors of the deflection and bending moment of the two-span rectangular plate with h/L=0.01
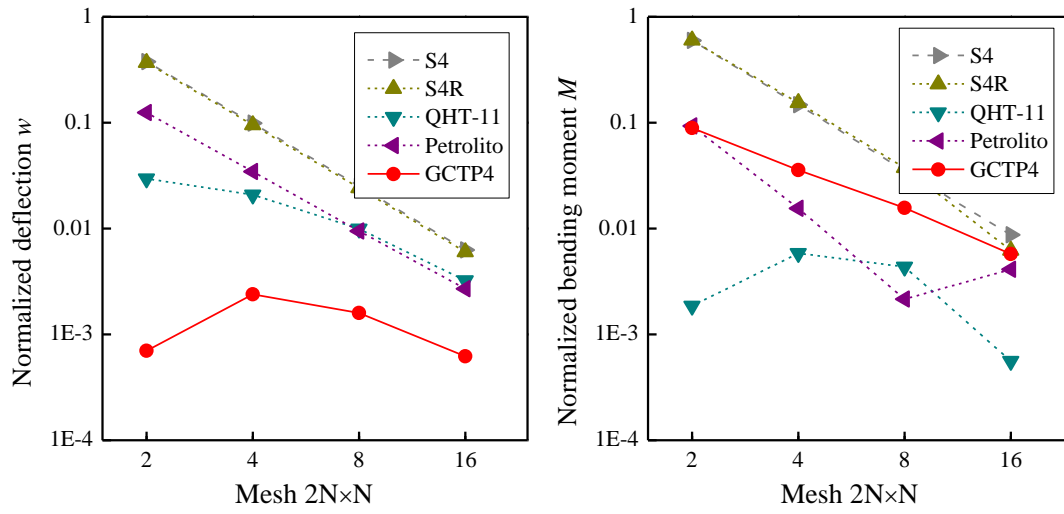
Figure 14. The relative errors of the deflection and bending moment of the
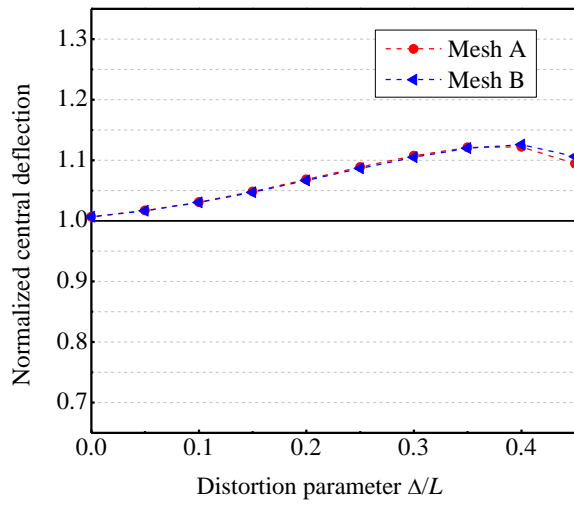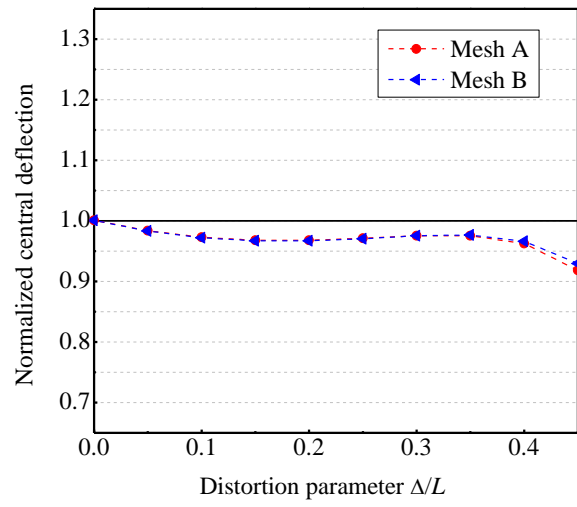two-span rectangular plate with h/L=0.1
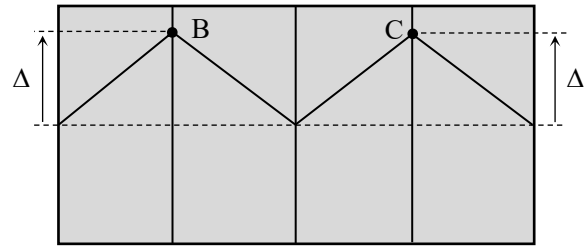
(a) Distorted mesh A
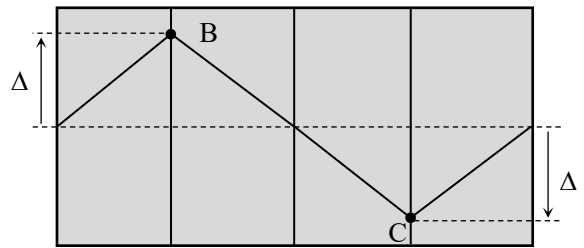
(b) Distorted mesh B

Figure 15. Two distorted meshes containing 4×2 elements for the two-span plate

(a) *h/L*=0.01

(b) *h/L*=0.1

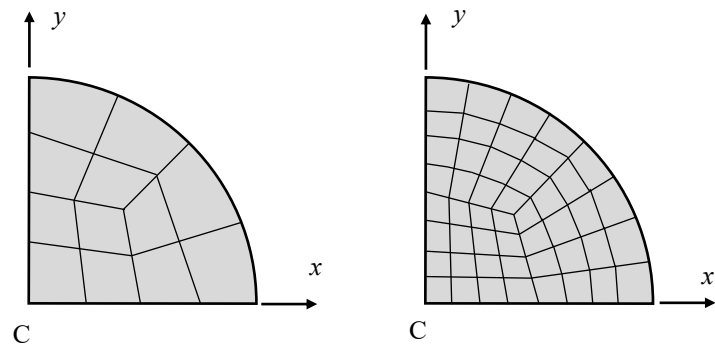Figure 16. The normalized deflection of the two-span plate versus the distortion parameter

Figure 17. The typical meshes for the circular plate